www.amlett.com, www.vbripress.com/aml, DOI: 10.5185/amlett.2014.10563 Published online by the VBRI press in 2014

Correlation between the pH value and properties of magnetite nanoparticles

Geeta Rana*, Umesh C. Johri

Department of Physics, G. B. Pant University of Agriculture & Technology, Pantnagar 263145, India

*Corresponding author. E-mail: ranawithgeeta@gmail.com

Received: 29 October 2013, Revised: 07 December 2013 and Accepted: 08 December 2013

ABSTRACT

Magnetite nanoparticles with particle size ~ 10 and 16 nm are synthesized by varying pH of the initial solution during chemical co-precipitation method. The X-ray diffraction patterns confirm the formation of spinel phase; however, the Raman spectra show an impure phase of antiferromagnetic Fe_2O_3 in the sample of smaller nanoparticles (10 nm). The cation distribution of these nanoparticles is estimated using the lattice parameter. Lower saturation magnetization of these samples, as compared to bulk, has been attributed to larger surface area of these samples. Same aspect has also been investigated from the optical band gap variation of these nanoparticles. Almost one third value of magnetization of smaller nanoparticles compared to larger one is due to the presence of Fe_2O_3 phase. The motive of the present study is to correlate the properties of magnetite nanoparticles with the synthesis parameters like pH and hence to tune them according to particular applications. Copyright © 2014 VBRI press.

Keywords: Magnetite nanoparticles; pH value; cation inversion; optical band gap.

Geeta Rana is working as Teaching Personnel in the Department of Physics, G. B. Pant University of Ag. & Technology, Pantnagar. She obtained her Ph. D. in 2011 from G. B. Pant University of Ag. & Technology, Pantnagar under the supervision of Dr. U. C. Johri. She has worked in the field of different ferrite nanoparticles.

Umesh C. Johri is working as Associate Professor in the Department of Physics, G. B. Pant University of Ag. & Technology, Pantnagar. He has completed his Ph. D. in 1989 from Indian Institute of Technology, Kanpur. He worked actively on different materials like glass, ceramics, magnetic materials and alloys. His current interests are quantum computation and quantum information.

Introduction

In the recent years, simple and reproducible methods to synthesize magnetic nanocrystals with desired shape and size have drawn considerable attention due to their unique size dependent properties such as magnetic, optical, electronic and surface, reactivity **[1]**. The correlation between the size, shape and properties of nanoparticles is not only important from fundamental physics point of view but also has technological importance in various fields such as biomedicine, optics and electronics. Among various applications, utilization of magnetic nanoparticles for biomedical applications is one of the most significant areas that are limited to the nanoparticles of small size along with magnetization value. In addition, the superparamagnetic behaviour is an added advantage for these applications. From last two decades, scientific community is committed for the development of nanoferrites for such applications. Among various ferrites, Fe_3O_4 seems to be the most suitable candidate for clinical applications due to the absence of any toxic element for biological tissues. It has been observed that magnetic properties are strongly dependent on the synthesis method and the parameters used during synthesis **[2]**. So, there is a strong need for the optimization of synthesis parameters to obtain nanoparticles having such properties that are useful in biomedical applications.

Magnetite Fe_3O_4, is one of the most useful industrial materials due to its excellent magnetic properties. It has cubic inverse spinel structure in which oxygen forms a face

centered cubic (FCC) closed packing and Fe ions occupy the interstitial tetrahedral (T) and octahedral (O) sites **[3].** For the system of ferrites, the distribution of cations over tetrahedral and octahedral sites can be expressed as **[4]-**

$$Me_{\gamma}Fe_{(1-\gamma)}[Me_{(1-\gamma)}Fe_{(1+\gamma)}]O_4$$

Here, the square brackets represent the ions at the octahedral sites; 'Me' is the divalent cation and γ is a constant which determine the cation distribution. For the present system $FeO.Fe_2O_3$ under consideration, the divalent cation is Fe and the cation distribution for this system can be expressed as –

$$(Fe^{2+}_{\gamma}Fe^{3+}_{(1-\gamma)})[Fe^{2+}_{(1-\gamma)}Fe^{3+}_{(1+\gamma)}]O_4$$

The electron hopping between Fe^{2+} and Fe^{3+} ions in the octahedral sites at room temperature, makes magnetite an important class of half-metallic materials. Several techniques have been used for the synthesis of iron oxide nanoparticles; however, co-precipitation method has been emerged as a better choice as it offers some advantages over other synthesis techniques like simple as well as a rapid preparation and one which provides an easy control on particle size. In co-precipitation method, all the reactions occur at the atomic scale which gives the final nanoparticles with high crystallization, stoichiometric composition and better homogeneity **[5]**. The main factors that affect the properties of the product in this method are pH of the precipitating medium and molarity of the starting precursors.

In the present work, we propose to study the effect of one of such effective parameters pH on the properties of magnetite nanoparticles. Variation of the pH value from 12 to 10 gives two samples with two different sizes. The difference in particle size leads to the modifications in various physical properties of these samples. A comparable study is made by techniques like X-ray diffraction (XRD), Fourier transform infrared spectroscopy (FTIR), Transmission electron microscopy (TEM), Raman spectroscopy, Vibrating sample magnetometer (VSM) and UV-Vis spectroscopy.

Experimental

Materials

For the synthesis of magnetite nanoparticles by chemical co-precipitation method, the starting chemicals $FeCl_2.4H_2O$, $FeCl_3.6H_2O$ and sodium hydroxide (NaOH) were purchased from Alfa Aesar (99.99 %, USA). The chemicals were of analytical grades and used without further purification.

Preparation of magnetite nanoparticles

In order to obtain the desired compositions, stoichiometric amounts of $FeCl_2.4H_2O$ and $FeCl_3.6H_2O$ were dissolved in ultra-pure water with constant stirring. The neutralization was carried out with 1.5M sodium hydroxide solution. The reaction temperature was kept at 85℃ for 45 minutes. The pH of the reaction was varied to obtain different samples of magnetite nanoparticles. To obtain the sample F_1 and sample F_2, the value of pH was kept at 12 and 10, respectively. Further any decrement in the initial pH value of the reaction was unable to precipitate the solution therefore, only two different pH values were used for this study. The precipitates were washed with distilled water to remove the sodium and chloride ions. The product was dried in a vacuum oven at a temperature of 70℃ for overnight to remove water contents. The dried powder was mixed homogeneously in a cleaned agate mortar and pestle **[6]**.

Characterizations

The X-ray diffraction pattern was obtained using Bruker AXS, D8 Advance, with Cu K_α (λ = 1.54 Å) radiation. The morphological studies of these samples were carried out using TECNAI 200 kV TEM and the magnetic properties were investigated using PAR 155 VSM. The Raman spectra were measured by Horiba JY HR800 micro-Raman system in unpolarized configuration. The optical properties of these samples were studied using UV-visible spectroscopy technique in Diffused Reflectance Mode.

Results and discussion

Involved reaction

The mechanism of the formation of Fe_3O_4 nanoparticles with ferrous and ferric salts in the ratio of 1:2, via 'co-precipitation' method is represented by equation 1. The stoichiometric amounts of ferrous and ferric ions react to produce Fe_3O_4;

$$Fe^{2+} + 2Fe^{3+} + 8OH^- \longrightarrow Fe_3O_4 + 4H_2O \quad (1)$$

The black precipitate appeared just after mixing the solution of iron salt with base solution of NaOH and it was concluded that the immediate co-precipitation of ferrous and ferric ions took place according to equation 1. An earlier study reveals that different phases of iron oxide are formed at different pH values of the initial solution **[7]**. The electron transfer between Fe^{2+} and Fe^{3+} plays a fundamental role in the crystallization process and a small proportion of Fe^{2+} ions (≥ 10 mol%) induces the crystallization of all the iron into spinel **[8]**.

Structure, size and morphological analysis

A typical XRD pattern of sample F_1 and F_2 is shown in **Fig. 1**. The broad peaks suggested the nanocrystalline nature of magnetite nanoparticles. For both samples, peaks obtained at (311), (220), (440), (400), (511) and (422) correspond to the inverse spinel structure of magnetite (JCPDS file # 19-0629). A small amount of NaCl is shown by few additional peaks in both samples which remain in the samples despite of several washings of precipitates. NaCl was formed due to the presence of Na^+ and Cl^- ions in the initial solutions **[9]**. The average crystallite size, estimated using Scherrer's formula **[6]**, was found 16±1 nm and 9±1 nm for F_1 and F_2, respectively. It confirmed that the crystallite size is smaller for smaller pH value that is relevant with previous studies **[1]**. Particle size of these samples, measured with TEM, was estimated ~ 16 and 10 nm, respectively (**Fig. 2**).

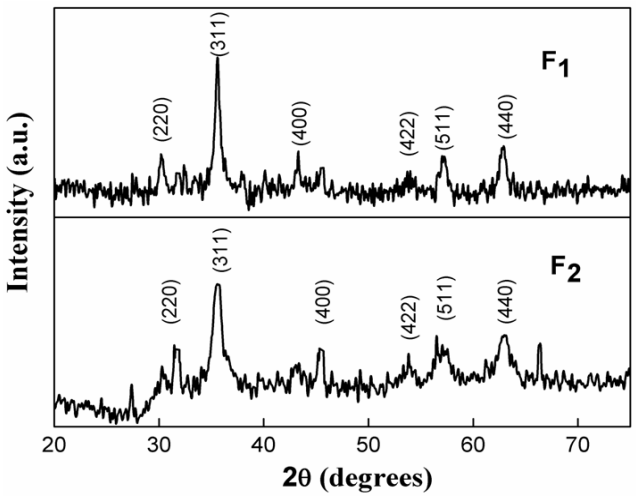

Fig. 1. XRD patterns for sample F_1 and F_2.

The important finding of the present work is the almost spherical shape and narrow size distribution of particles. The slight agglomeration in the TEM micrographs may be due to the Vander Waals forces and magnetic interaction between these magnetic nanoparticles. The Selected Area Diffraction (SAD) patterns (inset **Fig. 2**) also confirmed the inverse spinel structure of both the samples.

The spherical shape of these nanoparticles, shown from TEM study, motivated us to estimate the specific surface area which has been calculated using the formula **[6]**.

$$S = \frac{6000}{D\rho} \qquad (2)$$

where, D is the particle diameter and ρ is the X-ray density. Specific surface area for any material is the total surface area per unit of mass. The specific surface area for sample F_1 and F_2 was estimated 69.84 and 121.02 m^2/g, respectively. The increased specific surface area with the decrement in particles size may be correlated with the surface effects. As the particle size decreases, the surface to volume ratio increases and hence, the increased specific surface area was obtained.

Cation inversion

The unit cell parameter estimated for sample F_1 and F_2 is 8.358 Å and 8.360 Å, respectively. The reported value of unit cell parameter for bulk magnetite is 8.390 Å. The reduced value of lattice parameter for these samples, with respect to the bulk magnetite, leads a contraction in their unit cell **[1]**. This effect may be understood in terms of the relatively larger number of surface atoms than the atoms constituting the core of the nanoparticles. As the nanoparticles size decreases, the surface atoms will be relatively larger in number and the minimization of surface energy will necessitate the shrinking of the lattice, resulting into contraction. As an interesting result, despite of having higher surface energy for the smaller particle F_2, we observed a higher lattice parameter for it than that for the larger nanoparticles F_1. Here, for sample F_2 the reduction in particle size creates negative pressure on the lattice leading to a lattice cell volume expansion. Similar behavior has been reported earlier **[10-12]** for other oxide systems also. Shrinkage in unit cell will change the radii of tetra and octahedral site according to the relation **[13]**-

$$R_{tetra} = a\sqrt{3}(u - 0.25) - R_0 \qquad (3)$$

$$R_{octa} = a(0.625 - u) - R_o \qquad (4)$$

R_0 is the radius of oxygen ion (1.32Å), u is the oxygen parameter that is taken as 0.379 at room temperature 300 K **[14]** and 'a' is the lattice parameter estimated from the XRD pattern.

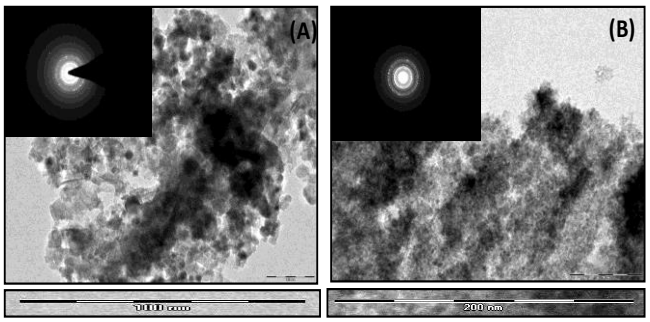

Fig. 2. TEM images and SAD patterns (inset) (A) sample F_1 (B) sample F_2.

On the other hand, the mean radius of the ions at tetrahedral site and octahedral site can also be written as-

$$R_{tetra} = \gamma r_{Fe}^{2+} + (1-\gamma) r_{Fe}^{3+} \qquad (5)$$

and the mean radius of the ions at the octahedral site is given by-

$$R_{octa} = \frac{1}{2}[(1-\gamma) r_{Fe}^{2+} + (1+\gamma) r_{Fe}^{3+}] \qquad (6)$$

As the two different values of lattice parameter are estimated earlier, two sets of the values of R_{tetra} and R_{octa} are obtained with the help of equations **(3)** and **(4)**. On solving **(5)** and **(6)**, g can be calculated and the cation distribution can be estimated. **Table 1** shows the estimated cation distribution for both samples. It clearly shows that, in the smaller particles, more amount of Fe^{2+} is shifting to the tetrahedral sites in comparison to the larger particles. Thus, higher degree of cation inversion is observed for the sample with smaller nanoparticles which is expected based on earlier reports **[15]**.

Table 1. Cation distribution for the samples F_1 and F_2.

pH	Particle size (nm)	R_{tetra} (Å)	R_{octa} (Å)	Cation Distribution	
				Tetrahedral site (T)	Octahedral Site (O)
12	16	0.547	0.548	$Fe^{2+}_{0.410}Fe^{3+}_{0.590}$	$Fe^{2+}_{0.590}Fe^{3+}_{1.410}$
10	10	0.736	0.737	$Fe^{2+}_{0.414}Fe^{3+}_{0.586}$	$Fe^{2+}_{0.586}Fe^{3+}_{1.41}$

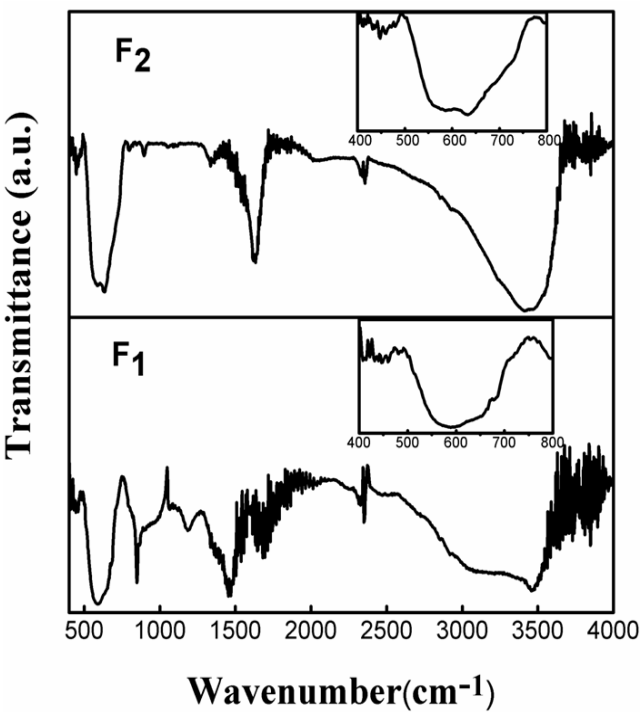

Fig. 3. FTIR spectra for sample F_1 and sample F_2, inset shows the FTIR spectra in the range of 400-800 cm^{-1}.

Table 2. Assignment of band position for sample F_1 and F_2 observed in FTIR.

Band Position (cm^{-1})		Band Assignment
F_1 (~16 nm)	F_2 (~10 nm)	
448	448	Octahedral site
592	607	Tetrahedral site
2354	2354	Atmospheric CO_2
1698	1630	H-O-H bending
3462	3422	H-O-H stretching

FTIR study

The FTIR spectra of these samples, shown in **Fig 3**, exhibit the bands corresponding to magnetite phase. For these samples of magnetite, we considered two ranges of the absorption bands, 400–4000 cm^{-1} and 400-800 cm^{-1} as suggested by earlier reports **[16]**. In ferrites, the band ~ 600 cm^{-1} is attributed to the stretching vibrations of the tetrahedral groups and that ~ 400 cm^{-1} corresponds to the octahedral groups. The assignment and comparison of modes is tabulated in **Table 2**. The shouldering of the band corresponding to the tetrahedral site is observed for both the samples. It is attributed to the Jahn-Teller's distortions produced by the Fe^{2+} ions that causes local deformations in the lattice owing to the non-cubic component of the crystal field potential, and hence lead to the splitting of this band, corresponding to the tetrahedral site **[17]**.

Raman study

The expected vibrational modes of the first Brillouin zone of magnetite (spinel structure) are given by **[18].**

$$\Gamma_{vib} = A_{1g}(R) + E_{1g}(R) + T_{1g} + 3T_{2g}(R) + 2A_{2u} + 2E_u + 4T_{1u}(IR) + 2T_{2u}$$

The modes T_{1g}, A_{2u}, E_u, and T_{2u} are optically silent, while modes $A_{1g} + E_g + 3T_{2g}$ are Raman active and the $4T_{1u}$ modes are infrared active. Analyses based on the quasi-molecular description of the spinel structure lead to the following description of normal mode motions of the FeO_4 tetrahedron: A_{1g}—symmetric stretch of oxygen atoms along Fe–O bonds, E_g and $T_{2g}(3)$—symmetric and asymmetric bonds of oxygen with respect to Fe, respectively, $T_{2g}(2)$—asymmetric stretch of Fe and O, $T_{2g}(1)$—translatory movement of the whole FeO_4 **[19]**. There are zero, or close-to-zero displacements of Fe atoms in modes A_{1g}, E_g, and T_{2g} **(3)**. All of these Raman modes are observed under ambient conditions. The presence of an inversion center in the centrosymmetrical space group *Fd3m* of magnetite implies the mutual exclusion of Raman and Infrared activities for the same vibrational modes. Raman peaks over the range of 460-660 cm^{-1} correspond to the modes of octahedral group (O-site) and those in the region of 660-720 cm^{-1} represent the modes of tetrahedral group (T-site) **[20]**.

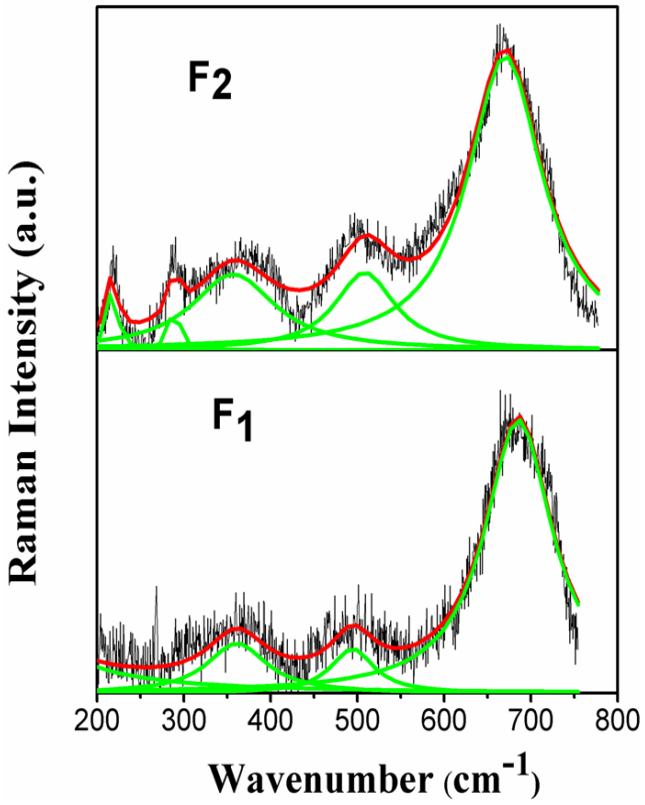

Fig. 4. Raman spectra for sample F_1 and F_2.

Table 3. Raman modes observed for sample F_1 and F_2.

Sample Name	Symmetry and Raman shift (cm^{-1})				
	T_{2g}		E_g	T_{2g}	A_{1g}
F_1	-	-	361	494	685
F_2	217	288	357	508	670

Fig. 4 shows the Raman spectra of the above samples. The observed Raman modes were fitted by Lorentzian function. Different Raman modes observed for both samples are shown in **Table 3**. There is a good match of peaks with the magnetite studied earlier **[21]**. Sample F_2 has two extra modes that did not appear in the spectrum of

sample F_1. For sample F_2, the mode at ~ 217 cm^{-1} is related to the magnetite itself while the presence of the peak at 288 cm^{-1} is studied earlier **[22]**. This peak suggests the beginning of oxidation that belongs to the characteristics signature of hematite and assigned as E_g **[23]**. The Raman scattering power of hematite is much higher than that for magnetite and even a very small amount of hematite causes the presence of spurious peaks in the Raman spectrum **[24]**. Thus, the slight presence of hematite in sample F_2, denoted by the peak at 288 cm^{-1}, may be a possible reason for its higher intensity in the Raman spectrum. The presence of hematite was not determined by the XRD results of sample F_2.

Another significant parameter of Raman signal, i.e. the bandwidth showed broadening for the smaller nanoparticles F_2. The broader peaks of F_2 suggests the reduced life time of phonons which is associated with an increased crystalline disorder in it. Usually, small particle size also causes a broadening of peaks. So this kind of broadening for sample F_2 with respect to sample F_1 also justifies the smaller size of F_2. We observed that the Raman shift for the sample F_2 is approaching towards the lower wavenumber. This red shift is possibly due to the optical phonon confinement effect **[25, 26]**. When the particle size reduces to the order of a few nanometers, the wave function of optical phonons will no longer be a plane wave. The localization of wave function leads to the phonon confinement effect which describes the phenomenon that occurs with the lifting of the phonon momentum selection rule $q \approx 0$, for the Raman scattering process within the ordered media.

Magnetic study

A visual inspection of hysteresis curves for these samples indicated drastic changes in their magnetic properties (**Fig. 5**). Sample F_1 exhibit coercive behavior; however, sample F_2 possesses extremely small values of coercivity and retentivity at room temperature and shows a superparamagnetic behavior. The superparamagnetism is due to the fact that below a certain critical particle size (<15 nm), a particle of ferromagnetic material would consist of a single magnetic domain. Since, both the curves did not saturate even up to a field of 10 kOe (**Fig. 5**); hence, saturation magnetization of these samples was estimated by fitting the field value (at higher values of the M-H curve) according to the equation **[27]**.

$$M = M_s (1\text{-}a/H) \qquad (7)$$

where, M_s is the saturation magnetization and 'a' is the fitting parameter. The intercept on M-axis gives the value of saturation magnetization. The saturation magnetization obtained for the sample F_1, using magnetization vs. 1/H curve, was 72.5 emu/g while for F_2 it was only 22.3 emu/g. The observed value of saturation magnetization for both samples is less than the reported value of bulk magnetite which is 92 emu/g **[28]**.

The huge reduction in the saturation magnetization for sample F_2 may be understood for various reasons. It has been mentioned elsewhere that magnetic properties of magnetite nanoparticle depend on the crystallinity **[29]**. Poor crystallinity leads to degradation in the magnetic properties; hence the low crystallinity of F_2 compared to F_1 may be one of the possible reasons for its reduced magnetization. The magnetization near the surface is generally lower than that in the interior which implies that magnetization decreases with reduction in size due to the prominent surface effects. The slight change in cation distribution may be another reason for the reduced magnetization value of smaller nanoparticles.

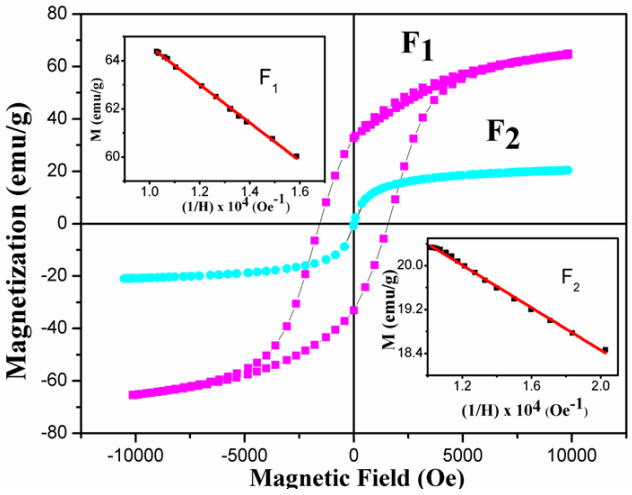

Fig. 5. Hysteresis curves for sample F_1 and F_2. Insets show the graph M vs. 1/H for both samples.

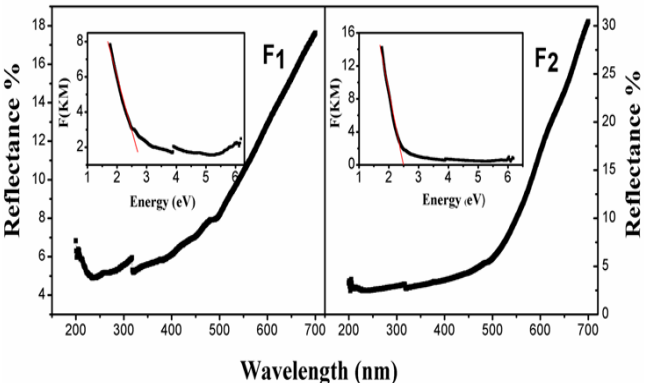

Fig. 6. Diffused Reflectance Spectra and K-M function plot (inset) for the sample F_1 and F_2.

The presence of hematite is also responsible for the lower value of saturation magnetization in sample F_2. Hematite is weekly ferromagnetic or antiferromagnetic system in nature **[30]**. As the magnetization of hematite is much less than that for magnetite hence, we obtained large reduction in the magnetization of sample F_2. Thus, the discussion of reduced magnetization of sample F_2 can be justified in the light of increased surface area, presence of hematite and low crystallinity.

Optical study

Fig. 6 shows the Diffused Reflectance spectrum of magnetite sample F_1 and F_2 in the range of 200 nm to 800 nm. Further, for the determination of optical band gap, we have plotted the Kubelka-Munk (K-M) function with the energy in inset of **Fig. 6 [31]**.

The energy corresponding to any wavelength can be determined using the formula

$$E = \frac{hc}{\lambda} = \frac{1237.5}{\lambda(nm)} \quad (8)$$

and the K-M function is defined as

$$F(R_\infty) = \frac{(1-R_\infty)^2}{2R_\infty} \quad (9)$$

where R_∞ is the limiting reflectance.

The most linear part of Energy vs. K-M function curve was fitted and the intercept on X-axis provided the value of optical band gap (**Table 4**).

Table 4. Optical band gap observed for sample F_1 and F_2.

Sample Name	Particle Size	Optical Band gap
F_1	16 nm	2.97 eV
F_2	10 nm	2.48 eV

Basically, the presence of a band gap is indicated by a sudden decrease in reflectance at a particular wavelength. Here, the band gap obtained for the smaller nanoparticles (sample F_2) is smaller than the band gap of larger nanoparticles (sample F_1). The band gap of nanosized materials is mainly associated with two factors: "quantum size effects" and "surface and interface effects" **[32]**. The quantum size effect leads to the blue shift or increase in E_g (band gap) with decrease in particle size while the surface and interface effects induces the red shift or decrease in E_g **[33]** on decreasing the particle size.

The earlier reported band gap for bulk magnetite is 0.15 eV **[34]**. The band gap estimated for sample F_1 and F_2 was 2.97 eV and 2.48 eV, respectively. For both the samples, an increased band gap was obtained with respect to the bulk magnetite which is in accordance with the quantum size effects. The smaller nanoparticles F_2 showed smaller band gap than that obtained for the larger nanoparticles F_1 which is attributed to the surface and interface effects. It is reported that below a particular crystallite size (<10 nm), surface and interface effects dominate over the blue shift factor hence the optical band gap decreases for the smaller crystallite size **[35]**. For the present case of smaller nanoparticles, the crystallite size falls under this cited limit hence, we obtained a red shift for smaller nanoparticles. Thus, it may be remarked that surface and interface effects are responsible for the reduction of band gap in sample F_2.

Conclusion

Synthesis parameter like pH value was found to be very crucial in deciding the various properties of magnetite nanoparticles. The crystallite size as well as particle size was increasing with the increment in pH value and all the physical properties were affected due to the size difference. Magnetite nanoparticles exhibit the attributes of cation distribution changes at nanodimensions. The direct consequence of this small degree of cation inversion may be considered as the reduced value of saturation magnetization for sample with lower pH and hence smaller particle size. The higher surface to volume ratio and superparamagnetic behavior of smaller magnetite nanoparticles were other reasons behind this reduction. The smaller nanoparticles with lower pH value indicated phonon confinement and dominancy of surface effects which were responsible for the red shift in Raman spectra and smaller band gap, respectively. The as-prepared magnetite nanoparticles with such small size and comparatively higher magnetization may be useful for biomedical applications.

Acknowledgements

Authors GR and UCJ are thankful to Prof. Ajay Gupta, Centre Director, Dr. T. Sripati, and Dr V.G. Sathe, UGC–DAE CSR, Indore, for providing experimental facilities. GR is grateful to Prof. O.N. Srivastava, BHU, Varanasi for providing the TEM facility. GR extends her warm thanks towards Dr. J.P. Singh, KEC Ghaziabad, for fruitful discussion.

Reference

1. Gnanaprakash, G.; Mahadevan. S.; Jayakumar, T.; Kalyanasundaram, P.; Philip, J.; Raj B. *Mater. Chem. Phys.* **2007**,103, 168. **DOI**: 10.1016/j.matchemphys.2007.02.011
2. Tartaj, P.; Morales, M. P.; Veintemillas-Verdaguer, S.; Carreno, T. G.; Serna, C. J. *J. Phys. D: Appl. Phys.* **2003**, 36, 182. **DOI**: 10.1088/0022-3727/36/13/202
   Patra, H. K.; Khaliq, N. U.; Romu, T.; Wiechec, E.; Borga, M.; Turner, A. P. F.; Tiwari, A. Advanced Healthcare Materials, **DOI**: 10.1002/adhm.201300225, **2013.**
   Tiwari, A. (Ed), In Advanced Healthcare Nanomaterials, WILEY-Scrivener, USA, **2014**.
3. Cornell, R. M.; Schwertmann, U. The Iron Oxide: Structure, Properties, Reactions, Occurrence and Uses, Wiley-Interscience, New York, 1996.
4. Yousif, A.; Elzain, M. E.; Mazen, S. A.; Sutherland, H. H.; Abdalla, M. H.; Manour, S. F. *J. Phys. Condens. Matter.* **1994**, 6, 5717. **DOI**: 10.1088/0953-8984/6/29/014
5. Fried, T., Shemer, G.; Markovich, G. *Adv. Mater*. **2001**, 13, 1161. **DOI**: 10.1002/1521-4095(200108)13
6. Rana, G.; Johri, U. C.; Asokan, K. *Euro. Phys. Lett.* **2013**, 103, 17008. **DOI**: 10.1209/0295-5075/103/17008
7. Faiyas, A. P. A.; Vinod, E. M.; Joseph, J.; Ganesan, R.; Pandey, R. K. *J. Magn. Magn. Mater.* **2012**, 322, 400. **DOI**: org/10.1016/j.jmmm.2009.09.064
8. Tronc, E.; Belleville, P.; Jolivet, J. P.; Livage, J. *Langmuir* **1992**, 8, 313. **DOI**: 10.1021/la00037a057
9. Ong, B. H.; Devaraj, N. K.; Matsumoto, M.; Abdullah, M. H. *Mater. Res. Soc. Symp. Proc.* **2008**, 1118, 56.
10. Gul, H.; Ahmed, W.; Maqsood, A.; *J. Magn. Magn. Mater.* **2008**, 320, 275. **DOI:** http://dx.doi.org/10.1016/j.jmmm.2007.05.032
11. Ayyub, P.; Palkar, V. R.; Chattopadhyay, S.; Multani, M. S. *Phys. Rev. B* **1995**, 51, 6135. **DOI**: 10.1103/PhysRevB.51.6135
12. Chattopadhyay, S.; Ayyub, P.; Palkar, V. R.; Multani, M. S. *Phys. Rev. B* **1995**, 52, 13177. **DOI**: 10.1103/PhysRevB.52.13177
13. Smit, J; Wijn, H. P. Ferrites, London, U.K.: Cleaver-Hume., 1995.
14. Nikolaev, V. I.; Shipilin, A. M.; Zakharova, I. N. *Crystallography Reports* **2001**, 46, 997. **DOI**: 10.1134/1.1420834
15. Chattopadhyay, P. P.; Nambissan, P. M. G.; Pabi, S. K.; Manna, I. *Phys. Rev. B* **2001**, 63, 054107. **DOI**: 10.1103/PhysRevB.63.054107

16. Murbe, J.; Rechtenbach, A.; Topfer, J. *Mater. Chem. Phys.* **2008**, 110, 426.
DOI: org/10.1016/j.matchemphys.2008.02.037
17. Mazen, S. A.; Abdallah, M. H.; Nakhla, R. I.; Metawe, H. F. *Mater. Chem. Phys.* **1993**, 34, 35.
DOI: org/10.1016/0254-0584(93)90116-4
18. Rana, G.; Johri, U. C. *J. Alloy. Comp.* **2013**, 577, 376.
DOI: org/10.1016/j.jallcom.2013.05.184
19. Shebanova, O. N.; Lazor, P. *J. Solid Stat. Chem.* **2003**, 174, 424.
DOI: 10.1016/S0022-4596(03)00294-9
20. Zhou, Z. H.; Wang Xue, J. M.; Chan H. S. O. *J. Mater. Chem.* **2001**, 11, 3110.
DOI: 10.1039/B105427A
21. Sousa, H. M.; Tourinho, A. F.; Rubim, C. J. *J. Raman. Spectrosc.* 2011, 31, 185. DOI: 10.1002/(SICI)1097-4555(200003)31
22. Dunnwald, J; Otto, A. *Corros. Sci.* **1989**, 29, 1167.
DOI: org/10.1016/0010-938X(89)90052-8
23. Shim, S. H.; Duffy, T. S. *Am. Mineral.* **2002**, 87, 318.
24. Shebanova, O. N.; Lazor, P. *J. Solid State Chem*. **2003**,174, 424.
DOI: *10.1016/S0022-4596(03)00294-9*
25. Singh, J. P.; Srivastava, R. C.; Agrawal, H. M.; Kumar, R. *J. Raman Spectrosc.* **2011**, 42, 1510. **DOI**: 10.1002/jrs.2902
26. Jubb, M.; Allen, H. C. *Am. Chem. Soc.* **2010**, 2, 2804.
DOI: 10.1021/am1004943
27. Ahn, Y.; Choi, E. J.; Kim, S.; An, D. H.; Kang, K. U.; Lee, B. G.; Baek, K. S.; Oak, H. N. *J. Kor. Phys. Soc.* **2002**, 41, 123.
28. Cullity, B. D. Introduction to magnetic materials, Reading: Addison-Wesley, 1972.
29. Wang, J.; Sun, J.; Sun, Q.; Chen, Q. *Mater. Res. Bull.* **2003**, 38, 1113. **DOI**: org/10.1016/S0025-5408(03)00129-6
30. Bodker, F.; Hansen, M. F.; Koch, C. B.; Lefmann, K.; Mørup, S. *Phys. Rev. B* **2000**, 61, 6826.
DOI: 10.1103/PhysRevB.61.6826
31. Tondon, S. P.; Gupta, J. P. *Phys. Status Solidi B* **1970**, 38, 363.
DOI: *10.1002/pssb.19700380136*
32. Kumar, P.; Malik, H. K.; Ghosh, A'; Thangavel, R.; Asokan, K.; *Appl. Phys. Lett.* **2013**, 102, 221903.
DOI: org/10.1063/1.4809575
33. Yuan, Z. H.; You, W.; Jia, J. H.; Zhang, Li-de *Chin. Phys. Lett.* **1998**,15, 535.
DOI: 10.1088/0256-307X/15/7/024
34. Gilbert, B.; Katz, J. E.; Denlinger, J. D.; Yin, Y.; Falcone, R.; Waychunas, G. A. *J. Phys. Chem. C* **2010**,114, 21994.
DOI: 10.1021/jp106919a
35. Singh, J. P.; Srivastava, R. C.; Agrawal, H. M. *AIP Conf Proc* **2010**, 1276,137.
DOI: org/10.1063/1.3504278

